

P1.8 DYNAMIC ADJUSTMENT WITHIN AN IDEALIZED NUMERICALLY-SIMULATED BOW ECHO: IMPLICATIONS FOR DATA ASSIMILATION

Ernani L. Nascimento* and Kelvin K. Droegemeier
School of Meteorology and Center for Analysis and Prediction of Storms
University of Oklahoma
Norman, Oklahoma 73019

1. INTRODUCTION

Recent investigations of Doppler radar data assimilation applied to convective storms have focused principally on isolated storms, such as supercells (e.g., Lin *et al* 1993, Crook and Sun 2001, Gao *et al* 2001, Weygandt *et al* 2001) and airmass thunderstorms (e.g., Sun and Crook 1998), or on sectorized regions along gust fronts (e.g., Xu *et al* 2001). However, a particular type of mesoscale convective system (MCS) remains to be investigated in the context of predictability and model initialization: the bow echo squall line (or simply, bow echo).

Similarly to supercells, bow echoes often display the remarkable characteristic of sustaining a coherent and persistent structure (though sometimes under weak mid-tropospheric forcing; Johns 1993). In contrast to supercells, however, the bow echo is an outflow-dominated MCS containing well-defined circulations in a broader scale (e.g., Weisman 1993). It therefore is possible that studies addressing the balances involved in and model sensitivity to observations of supercell storms (e.g., Weygandt *et al* 1999; Park and Droegemeier 2001) may not be entirely applicable to bow echoes.

To address this issue, we have conducted a numerical sensitivity analysis of an idealized bow echo with the primary goal of understanding how the dynamic (wind) and thermodynamic (temperature, pressure, moisture) fields — at both the scale of individual convective elements and the broader mesoscale — mutually adjust when one or more is perturbed. By understanding this adjustment, we hope to gain insight into which variables are most critical for storm-scale prediction, along with accuracy requirements for both observations and assimilation/retrieval.

2. METHODOLOGY AND CONTROL RUN

Our experiments utilize Version 4.5.1 of the Advanced Regional Prediction System (ARPS, Xue *et al* 2000) in an identical twin approach similar to that of Weygandt *et al* (1999). Specifically, a 6-hr control simulation of a bow echo, which serves as the "nature run" or "truth", is compared against several experiments in which selected variables in the control run are reset to their base state value at 4 hours (stable bow echo present in the control), *without any balancing*, following which is a 2-hr forecast. The evolution of the simulated bow echo from 4 to 6 hours in each case is then objectively and subjectively analyzed.

The model domain is 284 x 356 x 18.2 km³ with uniform horizontal and vertical grid spacings of 2 km and 400 m respectively. Convection is initiated by a +2 K thermal perturbation in the mixed layer. The vertical temperature and moisture profiles of the horizontally homogeneous environment follow Weisman and Klemp (1982), with a surface water vapor mixing ratio of 14 g kg⁻¹ and CAPE of approximately 2300 J kg⁻¹. The wind profile is that used by Weisman (1993), with 25 m s⁻¹ westerly vertical shear in the first 2.5 km and constant winds aloft. Ice microphysics (Lin *et al* 1983) and the Coriolis force are included, and the base state is geostrophically balanced, with the Coriolis force acting only on the wind perturbations.

Ideally, the lateral boundaries of all perturbation experiments should be forced, at each timestep, by the solution from the control simulation. For computational simplicity we avoid doing so, arguing that the 2-hr prediction time (i.e., from 4 to 6 hours) is sufficiently short, and the region of interest sufficiently removed from the boundaries, to render boundary effects of second order. Future experiments will be undertaken to verify this assumption.

Figures 1 and 2 show the control simulation from 4 to 6 hours. At 4-hr (the restarting time), the MCS displays characteristics of a classic bow echo squall line. The surface cold pool has spread primarily N-S, and a meso-high is clearly evident

* Corresponding author address:

Ernani L. Nascimento, School of Meteorology,
100 East Boyd, room 1310, Norman, OK 73019
e-mail address: nascimento@ou.edu

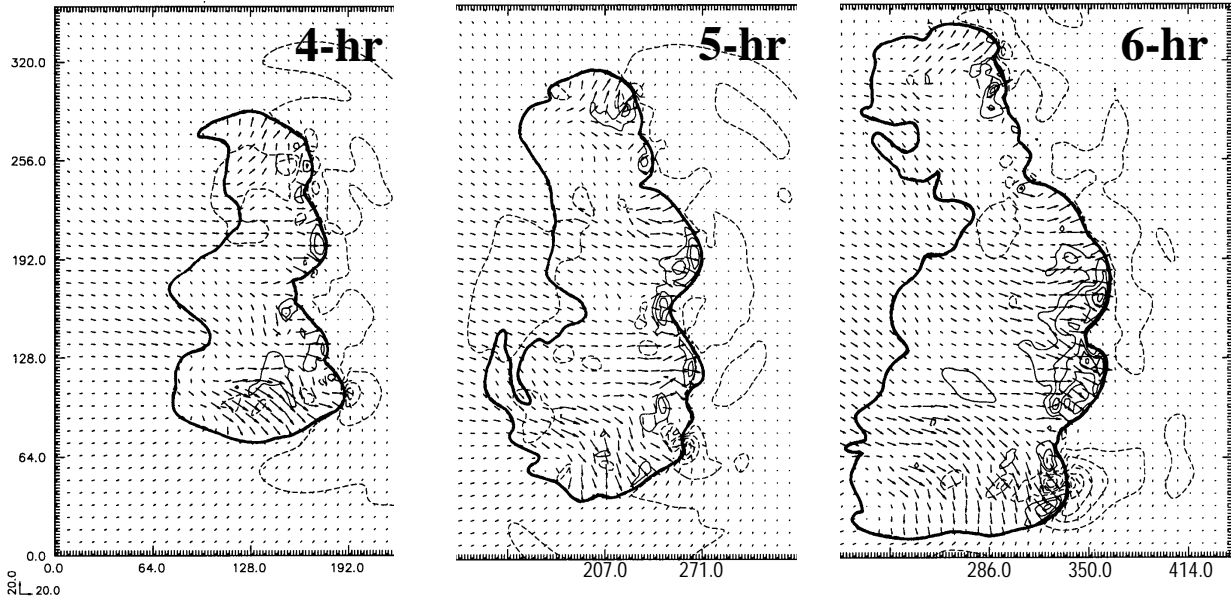


Figure 1: Time evolution of "surface" features ($z=200$ m): thick solid line denotes the -2 K potential temperature perturbation; pressure perturbation contours at each 100 Pa are indicated by thin solid (positive values) and dashed (negative values) lines. Vectors are ground-relative winds. Distances (from the origin at 4-hr) shown along the borders of the domain are in km.

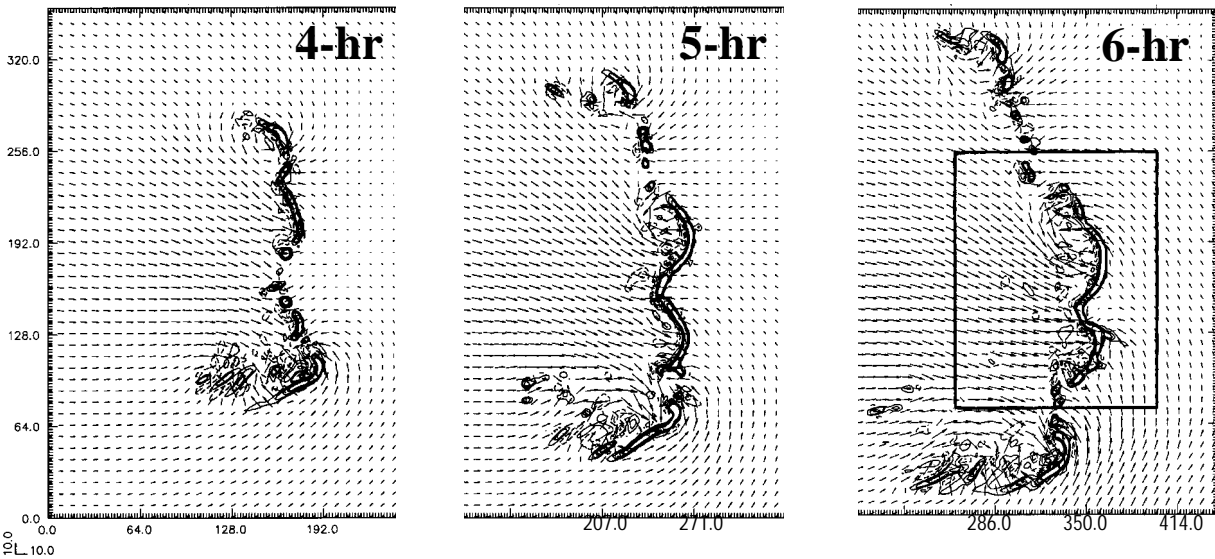


Figure 2: Storm features at $z=2600$ m: contours of vertical velocity perturbations indicated at each 2 m s^{-1} . Solid (dashed) lines are updrafts (downdrafts). Vectors are storm-relative winds. A domain speed of 22 m s^{-1} in the x -direction is applied from 4 to 6-hr, while an additional domain speed of -1.67 m s^{-1} in the y -direction is applied from 5 to 6-hr.

in the pressure field (figure 1). In this study the region of main interest is between $y=64$ km and 256 km where two major bow-echo segments develop (see, for example, figure 2, at 5 and 6-hr) accompanied by: (i) very well defined surface meso-high, (ii) derecho-like surface winds (i.e., reaching 25 m s^{-1} and higher), (iii) low- to mid-level rear to front flow characterizing a mesoscale jet (vertical cross-section not shown), (iv) well defined mesoscale convective (cyclonic) vortex (MCV) on the north end of the main bow echo (i.e., the one centered at $y=192$

km at 6-hr), (v) rear-inflow notches in the rain water mixing ratio field (not shown). These are storm features commonly observed with mature bow echoes (e.g., Przybylinski 1995).

Table 1 summarizes the set of sensitivity experiments, indicating the variables that are reset to their **base-state values** at the restart time (4 hours). For example, in experiment 1, the perturbation vertical velocity is set to zero (the base state) everywhere in the domain, while in experiment 2 the horizontal winds across the entire domain are set

equal to the background vertical profile. Therefore, the "signature" of the convective storm is eliminated for the variable being withheld, and the initial condition for that experiment becomes (artificially) unbalanced.

TABLE 1 - Summary of experiments restarting at 4-hr: variables that are set back to the base-state values.

Exper. 1	Vertical velocity (is eliminated) (w)
Exper. 2	Horizontal wind (V_H)
Exper. 3	Potential temperature (θ)
Exper. 4	Pressure (p)
Exper. 5	Water vapor mixing ratio (q_v)

As noted above, our goal is to understand how, and at what rates, the remaining fields adjust to the field that is withdrawn impulsively (similar in concept to geostrophic adjustment). For this we examine the time evolution of individual terms in the equations (to be shown at the conference) and also apply statistical error measures, such as the root-mean-square (RMS) error:

$$\text{RMS} = \sqrt{\frac{1}{M} \sum_{m=1}^M (F_m - C_m)^2}$$

where F is the "forecast" value from the sensitivity experiment, C is the corresponding value from the control run, and M is the total number of grid points in the domain. RMS errors are computed for several variables at 6-hr for the region of interest (indicated by a box in figure 2). By restricting our attention to this particular volume, we focus on the sector of the MCS that displays the most striking bow echo structure, and also reduce possible effects of the lateral boundaries (as noted above).

3. RESULTS

Figure 3 depicts the time series (data plotted at 5-min intervals) of the domain maximum updraft (DMU) for the control run and for each perturbation experiment. We note that the maximum updrafts obtained in the control experiment are stronger than in Weisman (1993), despite the fact that we use a background sounding with comparable CAPE and the same wind profile. The explanation likely involves our use of a finer vertical grid spacing, and our use of ice microphysics which tends to produce simulated storms having stronger updrafts (e.g., Johnson *et al* 1993).

During most of the simulation from 4 to 6-hr, the DMUs in the control run are in a quasi steady-state around 45 m s^{-1} , decreasing to 40 m s^{-1} only in the last 30-min of integration.

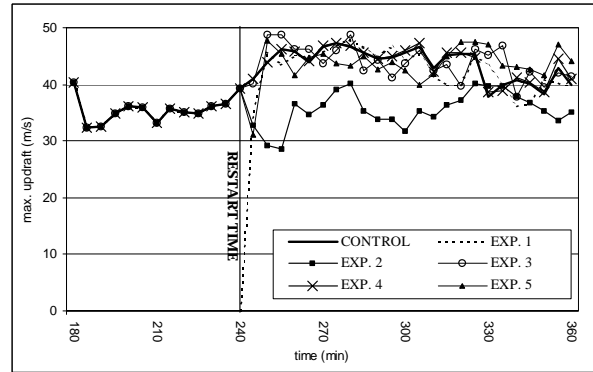


Figure 3: Time evolution (5-min intervals, from 3 to 6-hr) of domain maximum updraft.

It takes only ten minutes for the simulated storm in experiment 1 to restore its DMU, and the remaining evolution follows the control run with a good degree of agreement, especially in the first hour of integration. On the other hand, when withdrawing the perturbation horizontal winds (experiment 2), the simulation tends to significantly underestimate the DMUs. Since the horizontal length scale of the convective elements in the present simulation is much greater than the vertical scale, the updrafts are "wide" in aspect. In this case, updrafts can adjust to the horizontal wind field, as expected from an *acoustic adjustment* perspective (Fiedler 2001). Conversely, the updrafts cannot restore the horizontal wind field. This effect may account for the impact of experiment 1 not being so evident in terms of DMUs, while the elimination of perturbation horizontal winds led to an important modification in the time series of DMUs. Further analysis will be carried out to confirm this reasoning.

Figure 3 shows that the withdrawal of thermodynamic fields such as potential temperature perturbation (experiment 3) and water vapor mixing ratio perturbation (experiment 5) also caused relatively large deviations in DMUs. This result suggests that the knowledge of those thermodynamic fields is relevant in the model initialization process for the MCS "forecast", at least in terms of updraft strength. Since the MCS modifies the background environment by stabilizing the atmosphere (i.e., by consuming CAPE), the elimination of the perturbation potential temperature (experiment 3) allows the updrafts **in the MCS** to develop in a unmodified environment — in the early stages of the simulation — that is more unstable than the one in which the updrafts in the control run are embedded. This could explain the tendency for this simulation to overestimate the DMUs in the first half hour of integration.

In the case in which the water vapor mixing ratio is reset to the base-state (experiment 5), the initial drop in DMU (see figure 3) can be associated with the presence of an initially unmodified drier air in the mid- to high-levels of the storm. The unsaturated updrafts lose some of the momentum in the early stages of the integration due to the negatively buoyant air that is formed in association with enhanced evaporation and sublimation processes (recall that the mixing ratios of water and ice elements are kept unchanged). It seems that once the vertical distribution of latent heat release/absorption is restored, the updrafts regain their intensity. Additional analysis, to be shown in the conference, is needed to confirm the discussion above.

Figure 3 shows that not all thermodynamic fields are equally important to DMU. The withdrawal of the pressure perturbation field (experiment 4) led to a simulation in which the time series of DMU agreed remarkably well with the control run counterpart. This is because the pressure field recovers rapidly due to the mass continuity constraint.

Because DMUs analyzed above refer to the full 3D domain of the simulation, not all of those values necessarily lay within the main bow echo sector of the storm. Thus, RMS errors are calculated at 6-hr for the box indicated in figure 2. Within this (3D) box it is possible to find **all** mesoscale features associated with the major bow echoes, as described earlier. Table 2 summarizes the results.

TABLE 2 - RMS errors (t=6-hr)*

	EXP 1	EXP 2	EXP 3	EXP 4	EXP 5
θ (K)	1.45	2.42	2.08	0.50	2.51
p (Pa)	25.94	75.94	49.87	8.51	72.43
qv	0.36	0.87	0.64	0.09	0.78
qc	0.20	0.31	0.32	0.07	0.33
qr	0.36	0.67	0.57	0.10	0.65
qi	0.17	0.31	0.27	0.05	0.31
u	3.70	8.22	6.08	1.53	7.84
v	3.28	5.95	5.23	1.52	6.58
w	2.39	3.36	3.57	0.71	3.58

In general, the results indicated in table 2 agree fairly well with the analysis carried out with the time series of DMU. All variables studied display highest RMS errors with either experiment 2 or experiment 5 (note, though, that the RMS errors are not particularly high). At 6-hr, the highest RMS errors

* qc, qr, qi => cloud water, rain water, and cloud ice mixing ratios (in g kg^{-1}); u, v, w => zonal, meridional and vertical components of the wind (in m s^{-1}), respectively.

for variables p, qv, qr and u is with experiment 2, while experiment 5 yields the highest 6-hr RMS errors for θ , qc, v and w. For qi, the 6-hr RMS error is equally high for both experiments. Experiment 3 also leads to comparatively high values of RMS errors as expected from the previous discussion. Pressure perturbation withheld (experiment 4), on the other hand, produced the best forecast, with considerably low RMS errors at 6-hr. In fact, this run produced a bow echo storm that bears a remarkable resemblance with the control run.

Some additional statistics will be shown at the conference since the analysis of RMS errors alone (and at a single time) is not necessarily the best procedure to "verify" convective scale forecasts (Carr *et al* 1996). For now we choose to center most of our attention on the visual inspection of the numerical experiments in comparison with the control run. Figure 4 depicts the horizontal wind field and the "surface" cold pool (a and c) and low-level updrafts (b and d) at 6-hr for the runs in which the data contamination caused the greatest impact in the storm simulation, namely, experiments 2 and 5. This should be compared with figures 1 and 2 (at 6-hr).

When the horizontal winds are reset to their base state values (figs. 4a,b), the simulated storm is not capable of maintaining the bow echo structure and the north-south extension of the MCS is reduced. The "surface" winds, cold pool and meso-high are significantly weakened. The strong outflow seen in the center of the domain in the control run is not identifiable in figure 4a. The regions with maximum positive pressure perturbation (p') in the "surface" meso-high are reduced to a few areas with p' less than +200 Pa, while in the control run the meso-high covers a broader area in the center of the domain and maximum p' reaches +570 Pa.

Figure 4b shows that the horizontal distribution of the updrafts at the center of the domain is considerably modified (the qr field, not shown, is also modified). The mode of convection now is essentially multicellular and does not display a bow echo structure. The strong MCV present in the control run around $y=192$ km (see fig.2; 6-hr) is not reproduced in experiment 2. In addition, the rear-to-front flow is much weaker, not characterizing a mesoscale jet.

A close inspection of the first 30-min of simulation for experiment 2 (not shown) indicates that the updrafts are weakened in the sector of the MCS that should develop into the main bow echo segment. As a result, the hydrometeors subside as seen by the increase of low-level rain

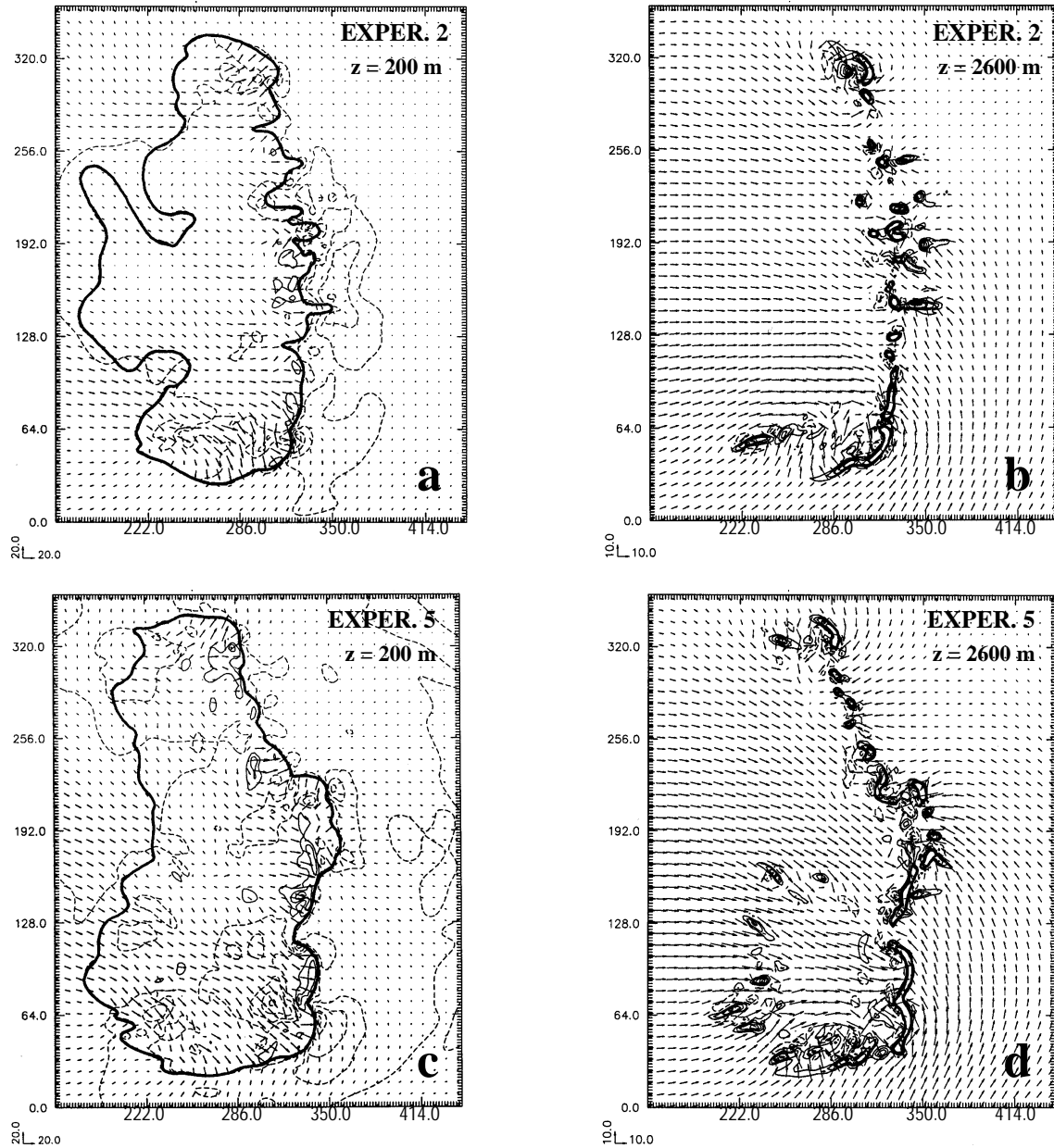


Figure 4: Storm features at 6-hr for experiments 2 (top) and 5 (bottom). (a) and (c): "surface" cold pool, ground-relative winds and pressure perturbation; (b) and (d) vertical motion and storm-relative (horizontal) winds. Contours just like in figures 1 and 2.

water mixing ratio accompanied by the reduction of mid- and upper-level hail, snow and cloud ice mixing ratios. These effects suggest that the latent-heat release mechanism is diminished in the mid-levels of the storm during the simulation. In fact, the θ' field shows less mid-level warming for experiment 2 than in the control run. The low- to mid-level meso-low that follows such warming and is, in part, responsible for the maintenance of a rear-to-front flow (Weisman 1993), tends to lag behind the weakening updrafts. The new mass distribution in the storm system affects the low-level pressure field and the outflow (surface meso-high) is not reestablished. In addition, the lack

of surface winds at the restart time slows down the forward motion of the cold pool.

Interestingly, the line-end outflow, to the north and south of the simulated MCS, is better recovered than the outflow in the center of the domain. We note that these line-end outflow regions are not associated with strong meso-highs. Further examination will be necessary to better understand the processes influencing such features.

Experiment 5 (fig. 4c,d) also fails to reproduce the main bow echoes in the center of the domain but, by 6-hr, some bulging segments in the line of storms are present further south. The strength of the

"surface" cold pool, meso-high and surface winds are stronger than for experiment 2, but weaker than in the control run. The shape of the leading edge of the cold pool does not show bow-shaped segments as in the control experiment. When resetting q_v field back to the base state, the lower levels in the MCS become moister than in the control simulation. This tends to reduce the evaporative cooling process in the sub-cloud layer, especially in the beginning of the simulation. Consequently, through hydrostatic considerations, the surface cold pool and meso-high are not as strong as in the control solution, weakening the outflow.

The low-level updrafts (fig. 4d) display a higher degree of organization when compared with experiment 2, and the rear-to-front flow is also stronger, but the simulation does not reproduce the control solution adequately. A smaller-scale bow echo is noted further south in the domain, including an incipient cyclonic MCV just south (west) of $y=128$ km ($x=350$ km). The processes that led to the development of this smaller-scale bow echo are still not clear, and will be investigated. The storm also produces more backbuilding activity in the southern half of the domain than the control solution. This is possibly due to a moister low-level atmosphere when the simulation was restarted with the basic-state value for q_v . These results emphasize the need of correctly initializing the water vapor field in the model initialization.

Not shown here are the results for experiments 1 and 4 which produce storms that closely resemble the control simulation, and experiment 3 that generates a slightly better "forecast" than experiments 2 and 5.

4. FINAL REMARKS

In general our preliminary results agree with some of the previous findings by Weygandt *et al* (1999) and Sun and Crook (2001) where they showed the importance of horizontal wind fields on the simulation of supercells. Among the variables examined, the withdrawal of perturbation pressure and vertical velocity fields at the restart time exerted the weakest impact on the simulation, while the contamination of water vapor mixing ratio and horizontal winds produced a poor "forecast" of the MCS.

It is important to notice that the use of an idealized thermodynamic sounding that does not include a low- to mid-tropospheric dry layer — as commonly observed with several bow echo cases — may have some influence in our results, since the strength of downdrafts can be partially modulated by this feature. In addition, results obtained from identical twin experiments have their own

weaknesses (e.g., not taking into account the impact of model errors).

The results shown here are preliminary and are only a first step in the broader context of convective-scale data assimilation applied to bow echoes. The understanding of the dynamic adjustment in the storm is a necessary step to assess the relative importance of different fields in the model initialization process. Some experiments under way include the elimination of low-level features not well monitored by typical weather radar systems (e.g., the cold pool). Radar data assimilation experiments will be carried out in a second stage of this research.

5. ACKNOWLEDGEMENTS

Funding for this research was provided by CNPq (Conselho Nacional de Desenvolvimento Científico e Tecnológico), Brazil, under grant number 201686/90-2, and by the National Science Foundation under grant ATM-9981130 to the second author. The publication is funded by Center for Analysis and Prediction of Storms (CAPS). Computer support was provided by the Environment Computer Applications System (ECAS) through CAPS.

6. REFERENCES

Complete list of bibliographical references can be found in the following web-page: <http://weather.ou.edu/~ernani/references.html>